

Localized Modes in the IR Phase of QCD

Andrei Alexandru,^{1,*} Ivan Horváth,^{2,3,†} and Neel Bhattacharyya^{4,‡}

¹The George Washington University, Washington, DC 20052, USA

²University of Kentucky, Lexington, KY 40506, USA

³Nuclear Physics Institute CAS, 25068 Řež (Prague), Czech Republic

⁴Poolesville High School, 17501 W Willard Rd, Poolesville, MD 20837, USA
(Dated: Dec 5, 2023)

Infrared (IR) dimension function $d_{\text{IR}}(\lambda)$ characterizes the space effectively utilized by QCD quarks at Dirac scale λ , and indirectly the space occupied by glue fields. It was proposed that its non-analytic behavior in thermal *infrared phase* reflects the separation of QCD system into an IR component and an independent bulk. Here we study the “plateau modes” in IR component, whose dimensional properties were puzzling. Indeed, in the recent *metal-to-critical* scenario of transition to IR phase, this low-dimensional plateau connects the Anderson-like mobility edge $\lambda_{\text{IR}}=0$ in Dirac spectrum with mobility edges $\pm\lambda_A$. For this structure to be truly Anderson-like, plateau modes have to be exponentially localized, implying that both the effective distances $L_{\text{eff}} \propto L^\gamma$ and the effective volumes $V_{\text{eff}} \propto L^{d_{\text{IR}}}$ in these modes grow slower than any positive power of IR cutoff L . Although $\gamma=0$ was confirmed in the plateau, it was found that $d_{\text{IR}} \approx 1$. Here we apply the recently proposed *multidimension* technique to the problem. We conclude that a plateau mode of pure-gluon QCD at UV cutoff $a=0.085$ fm occupies a subvolume of IR dimension zero with probability at least 0.9999, substantiating this aspect of metal-to-critical scenario to a respective degree.

Keywords: IR phase, QCD phase transition, quark-gluon plasma, Anderson localization, scale invariance

1. Introduction. Recent developments in thermal QCD [1–3], enabled by studies of lattice-regularized systems, led to a remarkable alignment of two seemingly unrelated aspects: the recently proposed infrared (IR) phase [1], and the older suggestion of Anderson-like localization in Dirac spectra [4–7].

This fusion arose via two new elements. The first one is the notion of *effective counting dimension* [8–10] characterizing probability measures constructed via discrete regularizations. This was adopted as a tool to describe IR and UV properties of quantum states or Dirac modes in terms of spatial dimensions d_{IR} and d_{UV} respectively [2]. The second element is the proposal of Ref. [3], *metal-to-critical scenario*, that QCD in IR phase features in fact two types of Anderson-like mobility edges: in addition to previously known $\pm\lambda_A$ ($\lambda_A > 0$) [6, 7], there is also a strictly IR mobility edge at $\lambda_{\text{IR}}=0$ [3]. To visualize the situation, top left panel in Fig. 1 shows the standard phase diagram of Anderson models in $E-W$ (energy – disorder strength) plane. Here the region enclosed by red solid line of critical points contains extended states. The QCD analogue is in the bottom left panel, showing the critical lines in $\lambda-T$ (Dirac eigenvalue – temperature) plane [3]. Note the extra line $\lambda_{\text{IR}}(T) \equiv 0$, $T_{\text{IR}} \leq T \leq T_{\text{UV}}$, where T_{IR} marks the transition to IR phase. The region enclosed by critical lines contains localized modes in this case. Hence, the relationship between QCD and Anderson situations is of dual rather than direct nature.

The rationale for d_{IR} is that it properly characterizes the physical space effectively occupied by electrons/quarks in various regimes. Indeed, it is based on effective counting [10] which is additive and thus defines meaningful spatial volumes (measures). This is not the case for gener-

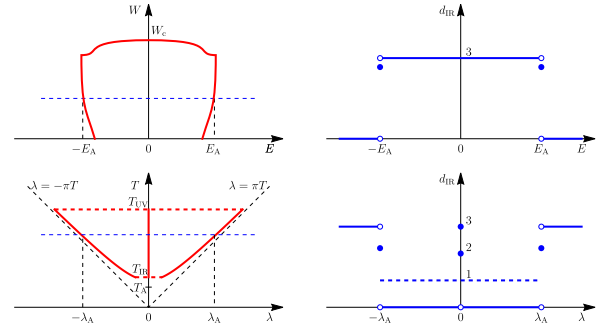


FIG. 1. Phase diagrams of localization in Anderson models (top) and QCD in IR phase (bottom). In Anderson case, E_A is the critical energy at given disorder strength W . In QCD case [3], T_{UV} denotes the possible endpoint of IR phase (onset of perturbative regime), and T_A the crossover temperature, both defined in Ref. [1]. See text for other explanations.

alized dimensions, such as frequently used D_2 . Dimension d_{IR} also conveniently identifies critical lines as collections of points where $d_{\text{IR}}(E, W)$ or $d_{\text{IR}}(\lambda, T)$ are non-analytic. The (E, W) setup defines critical features of Anderson localization phenomenon [11, 12], and known aspects of d_{IR} in this case are as follows [13–15]. In extended regime, $d_{\text{IR}} = 3$ is expected, which was confirmed numerically to very high accuracy [13]. It was also determined that $d_{\text{IR}} \approx 8/3$ at Anderson criticality irrespective of the universality class [13]. The value of d_{IR} and the degree of superuniversality are claimed to about 2-3 parts per mill.¹

¹ The expression for d_{IR} in terms of multifractal spectrum has recently been proposed and slightly higher value $d_{\text{IR}} = 2.733(3)$ (orthogonal class) based on it was suggested [16] but questioned in [17, 18].

Localized wave functions are expected to be bounded by a decaying exponential, which yields $d_{\text{IR}}=0$. While this last aspect is not fully guaranteed (exponential localization is not rigorously proved in 3 dimensions), the top right panel of Fig. 1 shows the present-day picture of generic $d_{\text{IR}}(E)$ for $0 < W < W_c$.

For Dirac spectrum in IR phase of QCD to be truly Anderson-like, the values of d_{IR} in corresponding regimes need to match the above. Conversely, the nature of differences, if any, should be clarified. In the bottom right panel of Fig. 1 we show the generic $d_{\text{IR}}(\lambda)$ for $T_{\text{IR}} < T < T_{\text{UV}}$ obtained in the pure-gluon QCD analysis of Ref. [2]. In the presumed localized regime $(-\lambda_A, 0) \cup (0, \lambda_A)$, $d_{\text{IR}} \approx 1$ was found (dotted line) instead of the expected $d_{\text{IR}} \approx 0$. Here we resolve this discrepancy. In Sec. 2 we perform the first direct calculation of d_{IR} in the Anderson localized regime and compare it to that in QCD. Similar behaviors are found with very slow decrease of d_{IR} estimates toward $L \rightarrow \infty$ limit. We attribute this to the logarithmic growth of effective volume for pure exponential which yields $d_{\text{IR}}=0$ but slow $L \rightarrow \infty$ convergence. The observed QCD-Anderson similarities then suggest that $d_{\text{IR}}=0$ in both cases. In Sec. 3 we perform the first *multidimensional analysis* [15] of both Anderson-localized states and QCD-localized Dirac modes, which makes a clear case that the two are indeed dimensionally equivalent.

2. Direct Evaluation. IR dimension d_{IR} is a leading power of linear size L ($L \rightarrow \infty$) in average effective volume $\langle \mathcal{N}_\star[\psi] \rangle_{L,\lambda} \propto L^{d_{\text{IR}}(\lambda)}$. Here ψ denotes Dirac eigenmodes $D\psi(x) = i\lambda\psi(x)$ or Anderson states at given energy. A useful concept is the finite-volume IR dimension [13]

$$d_{\text{IR}}(L, s) \equiv \frac{1}{\ln(s)} \ln \frac{\langle \mathcal{N}_\star \rangle_L}{\langle \mathcal{N}_\star \rangle_{L/s}}, \quad \lim_{L \rightarrow \infty} d_{\text{IR}}(L, s) = d_{\text{IR}} \quad (1)$$

with any $0 < s \neq 1$. If $P = (p_1, p_2, \dots, p_N)$, $p_i \equiv \psi^\dagger \psi(x_i)$ are probabilities entailed by ψ , then [9]

$$\mathcal{N}_\star[\psi] \equiv \mathcal{N}_\star[P] = \sum_{i=1}^N \min\{Np_i, 1\}. \quad (2)$$

As a first step in making the case for $d_{\text{IR}}=0$ of QCD plateau modes we compare their $d_{\text{IR}}(L, s)$ to that in a

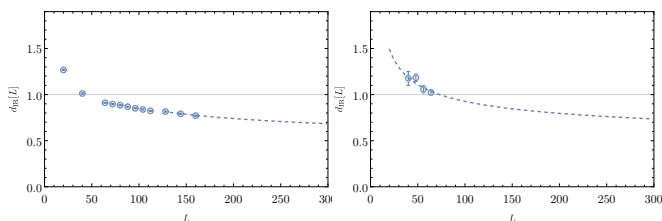


FIG. 2. Function $d_{\text{IR}}(L) \equiv d_{\text{IR}}(L, 2)$ in the Anderson model (O-class) at $W = 32$ (left panel) and “plateau modes” in IR phase of pure-gluon QCD. The dashed line, used to guide the eye, corresponds to a fit of the form $\langle \mathcal{N}_\star \rangle_L \sim [\log(L)]^k$. The effective size ℓ [3] of modes is $\ell \approx 2.9$ in the Anderson and $\ell \approx 5.2$ in the QCD case.

generic Anderson model. The Hamiltonian of the latter is (O class, periodic boundary conditions)

$$\mathcal{H} = \sum_r \epsilon_r c_r^\dagger c_r + \sum_{r,j} c_r^\dagger c_{r-e_j} + h.c. \quad (3)$$

where $r = (x_1, x_2, x_3)$ are lattice sites, e_j ($j=1, 2, 3$) unit lattice vectors, $\epsilon_r \in [-W/2, +W/2]$ uniformly distributed random potentials, and c_r the electron operators. We focus on 1-particle states in the vicinity of zero E (energy) at $W = 32$, which is deeply in the localized regime [19]. Note that $\langle \dots \rangle$ in Eq. (1) refers to disorder average in this case. For QCD it is the path-integral average.

In Fig. 2 we show results for $d_{\text{IR}}(L) \equiv d_{\text{IR}}(L, s = 2)$. The left panel features Anderson data at L up to 160. JADAMILU package [20] was used to perform the numerical diagonalization. The right panel shows the analogous data at available volumes of pure-gluon QCD in the IR-phase setup of Ref. [2], i.e. $T = 1.12 T_{\text{IR}}$, Wilson action at $\beta = 6.054$ ($a = 0.085$ fm, $r_0 = 0.5$ fm), $N_t = 1/(Ta) = 7$. Eigenmodes of the overlap operator ($\rho = 26/19$) were computed and analyzed on systems with sizes up to $L = 72$. Numerical implementation is described in Refs. [21–23]. We used modes in the eigenvalue range $\lambda \in (150, 450)$ MeV which is safely inside the plateau region [2].

Fig. 2 reveals similar dimensional behaviors in the two cases, with $d_{\text{IR}}(L) \approx 1$ in the region of accessible QCD sizes, and subsequent slow decrease toward the infrared in the Anderson case. Hence, the two nominally very different dynamics can indeed have a common Anderson-localization origin. Since there is little doubt that $d_{\text{IR}}=0$ in Anderson case, one expects the same in QCD. Also, for decaying exponential of width σ , it is easy to show that the leading $L \rightarrow \infty$ term in $\mathcal{N}_\star(L)$ is proportional to $\log^3(L/\sigma)$. It is this type of behavior that likely causes the slow decrease of $d_{\text{IR}}(L)$.

3. Multidimensional Analysis. While the above makes $d_{\text{IR}}=0$ for QCD plateau modes in IR phase plausible, convincing demonstration of dimensional equivalence to localized Anderson states is essential. We will show that the recently developed *multidimensional analysis* [15] (MDA) provides what is needed.

MDA aims to resolve the dimensional substructure (if any) in a probability measure defined by a discrete (e.g. lattice) regularization. It is conceptually different from effective counting dimensions (e.g. d_{IR}): rather than defining an *effective subset* of sample space and specifying its dimension, MDA considers a family of ordinary fixed subsets containing points with similar probabilities. Scaling properties of their volumes can reveal the presence of distinct dimensions. MDA differs from multifractal formalism [24] in that it focuses on physically relevant populations, namely those whose volumes contain nonzero total probability in $L \rightarrow \infty$ limit (See also Ref. [18].).

Given Anderson states ψ , MDA first orders probabilities in vectors $P[\psi]$ via $p_1 \geq p_2 \geq \dots \geq p_{N(L)}$. Closeness

within P then generically entails closeness of probabilities, and “populations” are defined by suitable sequential segments in P . To that end, vector (q_0, q_1, \dots, q_N) of cumulative probabilities is formed, namely $q_0 = 0$, $q_j = q_{j-1} + p(j)$, and function $\nu(q)$ of cumulative counts, namely $\nu(0) = 0$, $\nu(1) = N$, $\nu(q) = j(q) + (q - q_j)/(q_{j+1} - q_j)$ for $0 < q < 1$, is constructed. Here $j(q)$, $q \in (0, 1)$ is the largest j such that $q_j < q$. Clearly, $\nu(q)$ is the number of spatial points with largest probabilities, summing up to q . Their collection $\mathcal{S}(q)$ is a subset of lattice space. MDA then defines

$$d(q) := \dim \mathcal{S}(q) \quad \text{i.e.} \quad \nu(q, L) \propto L^{d(q)} \quad \text{for } L \rightarrow \infty \quad (4)$$

Given the order in P , $\nu(q)$ is increasing and convex, and $d(q)$ is non-decreasing [15]. Hence, $d(q)$ also arises “differentially” as dimension of $\sigma(q, \epsilon) := \mathcal{S}(q) \setminus \mathcal{S}(q - \epsilon)$ ²

$$\nu(q, L) - \nu(q - \epsilon, L) \propto L^{d(q, \epsilon)} \quad , \quad d(q, \epsilon) = d(q) \quad (5)$$

for all $0 < \epsilon < q$. This allows for *dimensional decomposition* of lattice space \mathcal{L} , and well-defined occurrence probabilities for all dimensions [15]. To that end, MDA partitions interval $[0, 1]$ into B equal parts of width $\epsilon_B = 1/B$, thus defining B -tuple of q -values $q_b = b/B$, $b = 1, \dots, B$. Then $\mathcal{L}(L) = \cup_{b=1}^B \sigma(q_b, \epsilon_B, L)$ and

$$N(L) = \sum_{b=1}^B v(q_b, \epsilon_B, L) L^{d(q_b, \epsilon_B, L)} \quad (6)$$

with finite-volume d and v introduced via [13, 15]

$$d(q, \epsilon, L) = \frac{1}{\log s} \log \frac{\nu(q, L) - \nu(q - \epsilon, L)}{\nu(q, L/s) - \nu(q - \epsilon, L/s)} \quad (7)$$

($0 < s \neq 1$) and $v(q, \epsilon, L) L^{d(q, \epsilon, L)} = \nu(q, L) - \nu(q - \epsilon, L)$. Relation (6) is exact at each B , and defines formal expressions such as $N(L) = \int_0^1 dq v(q, L) L^{d(q, L)}$. In a setup with suitable B (thus ϵ_B), Eq. (7) will be used here to estimate $d(q)$ since $\lim_{L \rightarrow \infty} d(q, \epsilon, L) = d(q)$ for all $0 < \epsilon < q$. Probability p of dimension d is $p(d) = \int_0^1 dq \delta(d - d(q))$ [15].

We described MDA using a sequence of states $\psi = \psi(L)$ labeled by increasing L , and the associated cumulative counts $\nu(q, L)$. However, all MDA calculations presented here are based on $\nu \rightarrow \langle \nu \rangle$, where $\langle \dots \rangle$ denotes the disorder average in Anderson case and the path-integral average in QCD case.

4. Plateau Modes. We now perform MDA of Anderson states (localized phase) and of QCD plateau modes (IR phase) using setups described in Sec. 2. Starting with the former, Fig. 3 (left) shows $d(q)$ calculated at $B = 10^3$ ($s = 2$) for increasing sizes L . Notice that q -dependences at each L already exhibit the monotonicity that is only guaranteed in $L \rightarrow \infty$ limit. From definition of $d(q)$ it

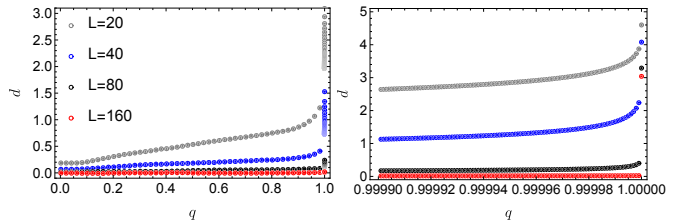


FIG. 3. Finite- L $d(q)$ in 3-d Anderson model (O-class) at $W=32$ ($s=2$). Left: calculation at $B=10^3$ (last shown bin is $b=B-1$). Right: calculation at $B=10^6$ (last bin is $b=B$).

follows that $d(1) = 3$. Hence, calculation at given B provides non-trivial information about $d(q)$ on the interval $[1/B, 1 - 1/B]$. Results for bin $b=1$ and $b=B-1$ (the first and the last data point shown for each L) correspond to these endpoint values. The key observation is that, while non-zero $d(q)$ do appear at finite L , they get quickly reduced as L increases. In the present case they effectively vanish at $L=160$.

The above provides numerical evidence that $d(q) = 0$ for $q \in (0, 0.999]$. However, it doesn’t exclude the possibility that higher dimensions appear with probability smaller than $\epsilon_B = 10^{-3}$. Indeed, this information is hidden within the last bin, i.e. the q -interval $(0.999, 1]$. To uncover its behavior, we divided it into another 10^3 sub-intervals, thus working at resolution $\epsilon_B = 10^{-6}$. Results for the right-most edge of q is shown in Fig. 3 (right), this time also including the last bin. Remarkably, non-zero dimensions again quickly scale out to zero for $q \leq 1 - 10^{-6}$. This is visible directly in $L = 160$ data before the $L \rightarrow \infty$ extrapolation. Notice that even the $q=1$ result (last bin) is already settled very near the correct value $d(1) = 3$.

To address the numerical rigor in the above, we show the $1/L \rightarrow 0$ extrapolations for $q = 1 - 10^{-6}$ (next to last bin) and $q = 1$ (last bin) in Fig. 4. The L -dependence was fitted to $d(q)$ plus general power using 5 largest values of L , and had excellent χ^2/dof . Note that $d(1)$ for the smallest (not fitted) lattice is significantly larger than dimension of the underlying space. This occurs because,

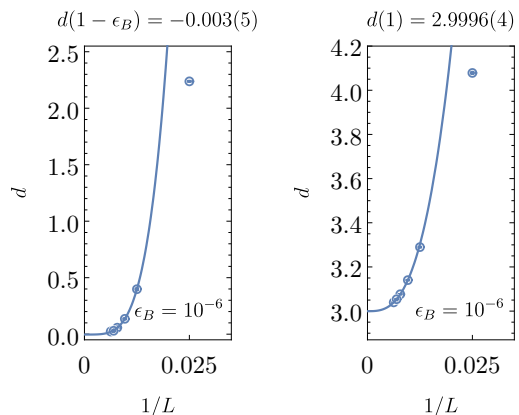


FIG. 4. Extrapolation ($L \rightarrow \infty$) of $d(q, \epsilon_B, L)$ for $q = 1 - \epsilon_B$ (left) and $q = 1$ (right) in 3-d Anderson model (O-class) at $W=32$. See text for details.

² Note that $d(q)$ represents the largest dimension present in $\mathcal{S}(q)$.

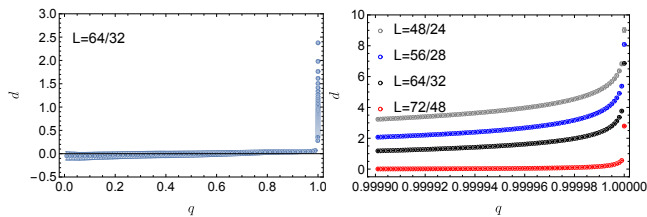


FIG. 5. Function $d(q, \epsilon_B, L)$ for QCD plateau modes. Left: at $B=10^3$ and $L=64$, $s=2$. Right: at $B=10^6$ and indicated pairs of L . The last shown bin is always $b=B-1$ ($q=1-\epsilon_B$).

by construction, the last bin has to accommodate all low- d populations whose total probability vanishes in thermodynamic limit. Such transport proceeds via a flow of volume toward the last bin at finite L , and results in an unphysically large finite- L dimension. Our results (indicated in Fig. 4) substantiate the conclusion that, for $E=0$ Anderson states at $W=32$ (O-class)

$$p(d) = (1 - \Delta) \delta(d) + \Delta \bar{p}(d) \quad , \quad \Delta < 10^{-6} \quad (8)$$

In other words, that the probability of encountering a non-zero spatial dimension (potentially featured in an unknown distribution $\bar{p}(d)$) is smaller than 10^{-6} .

Turning now to QCD in IR phase, we again work with plateau modes in the range $\lambda \in (150, 450)$ MeV [2]. In Fig. 5 (left) we show finite- L result at $L=64$ ($B=10^3$). Note that, even without an extrapolation, d is consistent with zero in almost the entire q -domain. To decipher the behavior at the very right edge where $d(q, L)$ rises, we again re-analyze the last bin using $B=10^6$. Results for various pairs of sizes are shown in Fig. 5 (right). Similarly to the Anderson case (Fig. 3 (right)), the rise gets quickly reduced as L increases, leaving behind yet narrower and weaker rise at $L=72$.

Statistical strength and the range of sizes in available QCD data is not sufficient to perform numerical analysis at $\epsilon_B=10^{-6}$ in the same way as in Anderson case (see Eq. (8)). Nevertheless, the point can be made convincingly here as well. To that end, we plot in Fig. 6 (left) average counts in the next-to-last bin ($q=1-\epsilon_B$, $\epsilon_B=10^{-6}$) and observe a tentative saturation involving the largest two systems $L=64, 72$. True saturation would imply that $d(q)=0$ for $q \leq 1-\epsilon_B$. Whether this is indeed taking place can be checked farther away from $q=1$ edge, where counts should saturate at smaller L . Fig. 6 (right) shows this for $q=0.9999$, revealing that a wider plateau is indeed formed. This leads us to propose that Eq. (8) in fact holds also in the QCD case.

5. Summary. While the notion of IR phase in QCD [1] was sparked by the IR behavior of Dirac spectral density $\rho(\lambda)$, it is the unusual effective spatial dimensions of Dirac modes [2], expressed by spectral function $d_{\text{IR}}(\lambda)$, that became a key element in understanding the phase and detecting it. Indeed, essential attributes of IR phase, namely the existence of deep IR fields [1, 25] and their

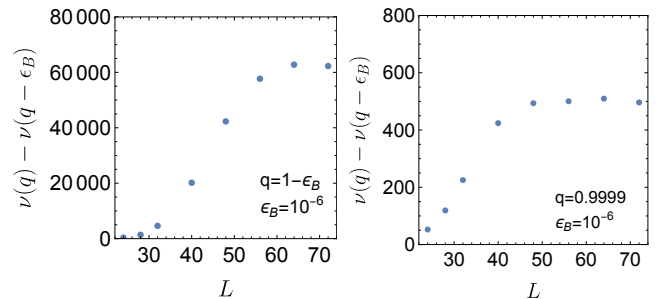


FIG. 6. Average counts $\nu(q) - \nu(q - \epsilon_B)$ in QCD plateau modes at $\epsilon_B=10^{-6}$ for $q=1-\epsilon_B$ (left) and $q=0.9999$ (right).

separation (decoupling) from the bulk [1], became natural in *metal-to-critical* picture of IR transition [3]. The underlying mechanism gives special role to Anderson-like critical points in Dirac spectra: the pair $\pm\lambda_A$, $\lambda_A > 0$ facilitates the decoupling, while $\lambda_{\text{IR}}=0$ governs the proposed long-range and possibly exactly scale-invariant physics of the IR component [1, 3]. Since Anderson critical points transform the space available to a particle by changing its dimension (see [13–15]), metal-to-critical scenario entails a specific discontinuous $d_{\text{IR}}(\lambda)$: a blueprint of IR phase.

However, evidence that produced [1–3] and later corroborated [26] the metal-to-critical scenario also generated an inconsistency. Indeed, the mechanism requires that plateau modes of IR phase (e.g. $\lambda_{\text{IR}} < \lambda < \lambda_A$) are exponentially localized, and thus of zero IR dimension. But the numerical evidence pointed toward $d_{\text{IR}} \approx 1$ instead. Here we resolved this issue by direct confrontation of Anderson-model data and QCD data, both in terms of d_{IR} and the new multidimensional technique function $d(q)$. Our analysis leaves little doubt that Anderson localized states and QCD plateau modes are dimensionally equivalent, both behaving as spatial probabilistic objects of IR dimension zero. This removes the above inconsistency.

We finally wish to convey four important points. (i) Summarizing the accumulated knowledge, we propose that the dimensional blueprint $d_{\text{IR}}(\lambda)$ of QCD in IR phase is shown in Fig. 7 (right). At the transition temperature T_{IR} , this non-analytic behavior replaces the constant $d_{\text{IR}}(\lambda)=3$ shown on the left. (ii) Strictly speaking, the extraordinary dimensional transformation at T_{IR} , represented by Fig. 7, has a robust numerical support in pure-gluon QCD. However, the results of recent extensive study [26] strongly suggest that, at least the structure

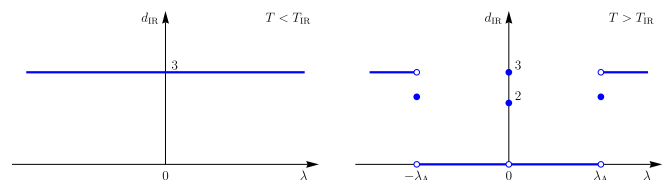


FIG. 7. Transition to QCD IR phase produces non-analyticity in $d_{\text{IR}}(\lambda)$, whose generic blueprint is shown on the right.

near $\lambda_{\text{IR}} = 0$ is also featured in “real-world” QCD. *(iii)* The previous comment applies to the entire QCD phase diagram in Fig. 1 (bottom left). While the multidimensional analysis has not yet been done in full-QCD case, the fact that the singularity structure at $\lambda_{\text{IR}} = 0$ is preserved [26] strongly suggests that the fate of the plateau is similar. Note also that dashing in $T = T_{\text{IR}}$ and $T = T_{\text{UV}}$ sections of critical lines expresses that these regions were not sufficiently studied yet, not even in pure-gluon QCD [3]. *(iv)* The precise meaning of d_{IR} at $\lambda_{\text{IR}} = 0$, represented in Fig. 7 (right) by two distinct values, is as follows. While $d_{\text{IR}}(0) \equiv \lim_{L \rightarrow \infty} d_{\text{IR}}(0, L) = 3$ is simply the IR dimension of exact zero-modes,

$$d_{\text{IR}}^+(0) \equiv \lim_{\epsilon \rightarrow 0} \lim_{L \rightarrow \infty} d_{\text{IR}}(0, \epsilon, L) \approx 2 \quad (9)$$

reflects the volume scaling of smallest non-zero modes. In Eq. (9) we introduced the notation $d_{\text{IR}}(\lambda_1, \lambda_2, L)$, where IR dimension is obtained from average N_* involving modes from the range $\lambda_1 < \lambda < \lambda_2$. Surprising results of Refs. [2, 26], support the indicated $d_{\text{IR}}^+(0) \neq d_{\text{IR}}(0^+)$.

A.A. is supported in part by the U.S. DOE Grant No. DE-FG02-95ER40907. I.H. acknowledges the discussions with Peter Markoš and his input on localization lengths.

* aalexan@gwu.edu

† ihorv2@g.uky.edu

‡ neel468167@gmail.com

- [1] A. Alexandru and I. Horváth, *Phys. Rev. D* **100**, 094507 (2019), arXiv:1906.08047 [hep-lat].
 [2] A. Alexandru and I. Horváth, *Phys. Rev. Lett.* **127**, 052303 (2021), arXiv:2103.05607 [hep-lat].
 [3] A. Alexandru and I. Horváth, *Phys. Lett. B* **833**, 137370 (2022), arXiv:2110.04833 [hep-lat].
 [4] A. M. Garcia-Garcia and J. C. Osborn, *Nucl. Phys. A* **770**, 141 (2006), arXiv:hep-lat/0512025.
 [5] A. M. Garcia-Garcia and J. C. Osborn, *Phys. Rev. D* **75**,

- 034503 (2007), arXiv:hep-lat/0611019.
 [6] T. G. Kovacs and F. Pittler, *Phys. Rev. Lett.* **105**, 192001 (2010), arXiv:1006.1205 [hep-lat].
 [7] M. Giordano, T. G. Kovacs, and F. Pittler, *Phys. Rev. Lett.* **112**, 102002 (2014), arXiv:1312.1179 [hep-lat].
 [8] I. Horváth, P. Markoš, and R. Mendris, *Entropy* **25**, 482 (2023), arXiv:2205.11520 [hep-lat].
 [9] I. Horváth and R. Mendris, *Entropy* **22**, 1273 (2020), arXiv:1807.03995 [quant-ph].
 [10] I. Horváth, *Quantum Rep.* **3**, 534 (2021), arXiv:1809.07249 [quant-ph].
 [11] P. W. Anderson, *Phys. Rev.* **109**, 1492 (1958).
 [12] P. W. Anderson, D. J. Thouless, E. Abrahams, and D. S. Fisher, *Phys. Rev. B* **22**, 3519 (1980).
 [13] I. Horváth and P. Markoš, *Phys. Rev. Lett.* **129**, 106601 (2022), arXiv:2110.11266 [cond-mat.dis-nn].
 [14] I. Horváth and P. Markoš, *Phys. Lett. A* **467**, 128735 (2023), arXiv:2207.13569 [cond-mat.dis-nn].
 [15] I. Horváth and P. Markoš, *Entropy* **25**, 1557 (2023), arXiv:2212.09806 [cond-mat.dis-nn].
 [16] I. S. Burmistrov, *Phys. Rev. Lett.* **131**, 139701 (2023).
 [17] I. Horváth and P. Markoš, *Phys. Rev. Lett.* **131**, 139702 (2023).
 [18] I. Horváth and P. Markoš, (2022), arXiv:2212.02912 [cond-mat.dis-nn].
 [19] P. Markoš, *Acta Physica Slovaca* **56**, 561 (2006).
 [20] M. Bollhöfer and Y. Notay, *Comp. Phys. Comm.* **177**, 951 (2007).
 [21] A. Alexandru, M. Lujan, C. Pelissier, B. Gamari, and F. X. Lee, in *Application Accelerators in High-Performance Computing (SAAHPC), 2011 Symposium on* (2011) pp. 123–130, arXiv:1106.4964 [hep-lat].
 [22] A. Alexandru, *Comput. Sci. Eng.* **17**, 14 (2014).
 [23] A. Alexandru, C. Pelissier, B. Gamari, and F. Lee, *J. Comput. Phys.* **231**, 1866 (2012), arXiv:1103.5103 [hep-lat].
 [24] T. C. Halsey, M. H. Jensen, L. P. Kadanoff, I. Procaccia, and B. I. Shraiman, *Phys. Rev. A* **33**, 1141 (1986).
 [25] A. Alexandru and I. Horváth, *Phys. Rev.* **D92**, 045038 (2015), arXiv:1502.07732 [hep-lat].
 [26] X.-L. Meng, P. Sun, A. Alexandru, I. Horváth, K.-F. Liu, G. Wang, and Y.-B. Yang (χ QCD, CLQCD), (2023), arXiv:2305.09459 [hep-lat].